GEOPHYSICS, VOL. 70, NO. 5 (SEPTEMBER-OCTOBER 2005); P. K39–K42, 3 FIGS.
10.1190/1.2049349

Letters

Effect of antennas on velocity estimates obtained from crosshole GPR data

James D. Irving[1] and Rosemary J. Knight[1]

ABSTRACT

To obtain tomographic images with the highest possible resolution from crosshole ground-penetrating radar (GPR) data, raypaths covering a wide range of angles between the boreholes are required. In practice, however, the inclusion of high-angle ray data in crosshole GPR inversions often leads to tomograms so dominated by inversion artifacts that they contain little reliable subsurface information. Here, we investigate the problems that arise from the standard assumption that all first-arriving energy travels directly between the centers of the antennas. Through numerical modeling, we show that this assumption is often incorrect at high transmitter-receiver angles and can lead to significant errors in tomographic velocity estimates when the antenna length is a significant fraction of the borehole spacing.

INTRODUCTION

Crosshole ground-penetrating radar (GPR) tomography is a popular method for high-resolution imaging of the shallow subsurface. Applications include determining the location of underground tunnels and voids (Moran and Greenfield, 1993), delineating orebodies (Fullagar et al., 2000), mapping fractures in bedrock (Olsson et al., 1992), and estimating subsurface lithology and hydrogeological properties using field- or laboratory-derived petrophysical relationships (Tronicke et al., 2004). The spatial resolution of tomographic images obtained from crosshole GPR data is a critical parameter that determines both the way in which the data are used and the value of the data for a specific application.

Of interest in our research is the use of GPR images to quantify the spatial variability of the subsurface for the purpose of predicting contaminant fate and transport. This application requires that our images have the best possible resolution in all directions. To obtain tomographic images with such high resolution from crosshole GPR data, raypaths covering a wide range of angles between the boreholes are required. This is a direct consequence of the Fourier projection-slice theorem, which states that each set of rays passing through an object at a particular angle (which constitutes a projection) yields one slice of that object's 2D Fourier spectrum (Rector and Washbourne, 1994). In practice, however, the inclusion of high-angle ray data in crosshole GPR inversions can be problematic (Peterson, 2001; Alumbaugh and Chang, 2002). That is, the inclusion of these data often results in tomograms so dominated by inversion artifacts that they contain little, if any, reliable subsurface information. For this reason, common practice is to limit the aperture of crosshole GPR data sets prior to inversion by discarding rays at angles greater than a particular threshold value (e.g., Alumbaugh and Chang, 2002).

The process of aperture limitation tends to yield reasonable tomographic images from crosshole GPR data. In our experience, however, it typically requires that we discard all rays at angles above 40° from the horizontal, which is often well below the maximum angle at which first-arrival data can be reliably picked. We are therefore degrading the potential resolution of our images by discarding these rays. We are interested in determining why the high-angle rays have such a negative effect on the images. Once this has been resolved, it may be possible to find a means of properly incorporating these data into crosshole GPR inversions.

In this study, we explore the idea that a key assumption, currently used in the inversion of all crosshole GPR data, is invalid for high-angle rays. Crosshole GPR inversion strategies treat the antennas as point sources and receivers whose

Manuscript received by the Editor March 21, 2005; revised manuscript received April 30, 2005; published online September 12, 2005.
[1]Stanford University, Department of Geophysics, Room 360, Mitchell Building, Stanford, California 94305-2215. E-mail: jdirving@pangea.stanford.edu; rknight@pangea.stanford.edu.

locations are given by the antenna midpoints. That is, these strategies effectively ignore the length of the antennas and assume that all first-arriving energy travels directly between the antenna centers. In many cases, however, the antenna length is a significant fraction of the separation distance between the boreholes. Here, we use numerical modeling to investigate whether, for large vertical offsets between the transmitter and receiver antennas, first-arriving energy can sometimes travel between the antenna tips.

VELOCITY ALONG A BOREHOLE GPR ANTENNA

A key parameter in assessing the travel path of electromagnetic (EM) waves in a crosshole GPR experiment is the velocity at which energy travels along the borehole antennas, v_{ant}, relative to the velocity of EM waves through the medium between the boreholes, v_{med}. Because the borehole antenna wires are not embedded within the earth in a crosshole GPR experiment, but rather are surrounded first by the antenna insulation and then the borehole-filling material, these two velocities are usually quite different. If $v_{ant} \leq v_{med}$, then the first-arriving energy at all transmitter-receiver angles should be that energy traveling directly between the antenna centers. In contrast, if $v_{ant} > v_{med}$, then the possibility exists at high transmitter-receiver angles for the first-arriving energy to travel between the tips of the antennas. More specifically, it is possible in this case that the first-arriving energy (1) travels from the center feed point along the transmitter antenna to the tip at velocity v_{ant}, (2) is radiated from the tip of the transmitter antenna, (3) travels through the subsurface at velocity v_{med}, (4) is received at the opposite tip of the receiver antenna, and (5) travels along the receiver antenna from the tip to the center input terminal at velocity v_{ant}.

The physics governing the propagation of energy along an insulated antenna in a borehole are very complex and involve solving Maxwell's equations in cylindrical coordinates subject to boundary conditions at the various interfaces surrounding the antenna wire. In general, the velocity of energy traveling along a borehole GPR antenna will be most sensitive to the material closest to the antenna wire (i.e., the antenna insulation) and less sensitive to material farther away. For an excellent treatment of the theory of insulated antennas, along with a derivation of the propagation constant on such an antenna under certain limiting assumptions, refer to King and Smith (1981) and King et al. (1983). Unfortunately, the assumptions required for the propagation-constant derivation are too restrictive for our purposes. We therefore determine the velocity of energy along a borehole GPR antenna using a numerical modeling approach.

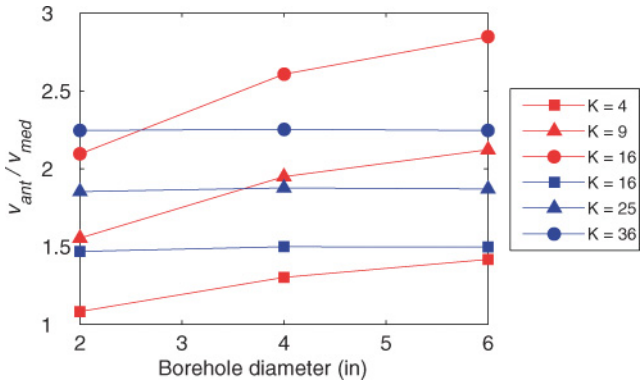

Figure 1. Antenna-to-medium velocity ratio (v_{ant}/v_{med}) determined versus borehole diameter for a number of cases in the vadose zone (red, air-filled borehole) and the saturated zone (blue, water-filled borehole). The κ values represent the dielectric constant of the medium surrounding the boreholes.

Figure 1 shows the ratio of the antenna velocity to external medium velocity (v_{ant}/v_{med}) that we calculated for a realistic borehole GPR antenna in a variety of vadose- and saturated-zone situations. To create this plot, we first constructed a finely discretized finite-difference time-domain (FDTD) model of the antenna and its immediate surroundings in 2D cylindrical coordinates, based on the approach presented by Holliger and Bergmann (2002). This model was then used to obtain the current distribution on the antenna during transmission when it was placed in air- and water-filled boreholes of various diameters. The boreholes were surrounded by media having different values of the dielectric constant κ. The antenna design used for the simulations was based on the borehole antennas in our commercial GPR system and consisted of a 5-mm-diameter copper cylinder with electrical conductivity $\sigma = 5 \times 10^7$ S/m, surrounded to a 30-mm-diameter by nonconductive insulation having $\kappa = 4$. To feed the antenna, we applied a Gaussian voltage pulse, having a -20 dB width of approximately 5 ns, to a 1-mm feed gap located at the center of the antenna wire. The antenna velocity was obtained by determining the first-arrival time of the resulting current pulse as it traveled to each point along the antenna.

As shown in Figure 1, v_{ant}/v_{med} is much more dependent upon borehole diameter in the vadose zone than in the saturated zone. This is because, in the case of a water-filled borehole, the borehole acts as a dielectric waveguide and thus the external medium has little influence on the velocity of energy along the antenna (Holliger and Bergmann, 2002). More important, however, is that for most of the cases considered, Figure 1 clearly shows v_{ant}/v_{med} to be significantly greater than one. Surprisingly, this is even the case in a water-filled borehole. The antenna insulation (a fast dielectric) is evidently thick enough to allow energy to propagate along the antenna at a velocity greater than that of the saturated external medium, despite being surrounded by water (a very slow dielectric). Figure 1 thus indicates that, for the insulated antenna we have considered, it is often possible at high transmitter-receiver angles for energy traveling between the tips of the antennas to arrive before energy traveling directly between their centers. In the next section, we evaluate the implications of this result for crosshole GPR tomography and find that significant errors in velocity estimates can occur when this phenomenon is not addressed.

CROSSHOLE GPR MODELING RESULTS

Homogeneous medium

We first consider a crosshole GPR experiment where the medium between the boreholes is homogeneous with $\kappa = 25$. This is a typical value of the dielectric constant for earth materials located in the saturated zone. We generate synthetic crosshole GPR data through this medium using finite-length

antennas. We then examine the errors that can result in velocity estimates obtained from the synthetic data when we assume that first-arriving energy always travels directly between the antenna centers.

To numerically simulate transmission and reception between realistic, finite-length borehole GPR antennas, we use a superposition of point dipole source and receiver responses in 2D cylindrical coordinates, which replicates the antenna current distribution obtained from detailed FDTD modeling. We have found that results obtained using this technique are in excellent agreement with analytical, field, and finely discretized numerical modeling results. Our modeling approach will be presented in an upcoming publication. For all of the examples in this study, we also simulated moderate resistive loading on the antennas such that the waveforms produced were similar to crosshole waveforms recorded with our commercial GPR system. Borehole GPR antennas tend to be resistively loaded, but only lightly, to obtain a compromise between a short radiated pulse and maximum power transfer into the ground.

Figure 2 shows the velocity error that results at different transmitter-receiver angles when we assume that first-arriving energy travels directly between the centers of the antennas. This error was determined using the following equation:

$$\%\ \text{error} = \frac{v_{meas} - v_{true}}{v_{true}} \times 100, \qquad (1)$$

where v_{meas} is the velocity measured from the synthetic data using the picked first-arrival time, and v_{true} is the known velocity of the medium between the boreholes (in this case, 0.06 m/ns).

We modeled a number of different cases corresponding to variations in v_{ant}/v_{med}, the borehole separation distance, and the length of the transmitter and receiver antennas. The flat-lying solid red curve in Figure 2 corresponds to the case where the velocity along the antennas was set equal to the velocity of the surrounding medium (i.e., $v_{ant}/v_{med} = 1$). As expected, there is no error in the measured velocity with angle. A very different behavior is observed, however, for all of the other curves shown in Figure 2. In these cases, there are no errors in the measured velocities for low propagation angles between the antennas, but errors clearly exist at higher angles as a result of our assumption that first-arriving energy travels directly between the antenna centers. For low transmitter-receiver angles, this assumption is valid. At higher angles, however, energy traveling between the antenna tips arrives first, which results in a measured velocity that is greater than the true velocity of the medium.

We now consider the magnitude of the errors in Figure 2. The green curve in the figure was created using a conservative antenna-to-medium velocity ratio of 1.5, 0.8-m-long antennas (which is the length of the 100-MHz antennas in our commercial borehole GPR system), and a borehole separation of 4 m. These parameters are typical of many crosshole GPR surveys and result in an error in velocity of 2% at some transmitter-receiver angles. As we see will in the next section, a consistent error of this magnitude can have significant effects on the tomograms obtained from crosshole GPR data. All of the other curves shown in Figure 2 represent a perturbation of one of the three parameters described above from the values used for the green curve. From these results, we see that the velocity error associated with high-angle rays is greatest for large values of v_{ant}/v_{med}, small borehole separations, and longer (i.e., lower frequency) antennas.

Heterogeneous medium

We now consider crosshole GPR data acquired through the heterogeneous medium shown in Figure 3a. This velocity model was constructed using the GSLIB geostatistical software package (Deutsch and Journel, 1992). A range of $20 \leq \kappa \leq 32$ was chosen to represent earth materials in the saturated zone. The boreholes located on either side of the model are 4 m apart and 12 m deep. The transmitter and receiver locations were spaced every 0.25 m down the boreholes from 0.5 to 11.5 m. To produce all of the tomograms for this example, we again assumed that all first-arriving energy travels directly between the antenna centers. In addition, straight rays were assumed in all of the inversions, and a Laplacian smoothness operator was used for regularization purposes. The same parameters were used in each inversion so that differences between the resulting tomograms could be fully attributed to differences between the antennas and apertures used.

We first generated synthetic crosshole data through the velocity model in Figure 3a using point dipole sources and receivers so that all first-arriving energy would truly travel between the antenna centers. This was done using the modeling approach of Holliger and Bergmann (2002) with a 100-MHz Ricker wavelet source function. Figure 3b shows the inversion result for the point source and receiver data using all available traveltimes, which involved rays at angles up to 70° from the horizontal. There is excellent agreement between Figure 3b and the true velocity model in Figure 3a as a result of the agreement between our forward model and inversion procedure on the path taken by first-arriving energy and the wide angular coverage provided by the data set.

We next generated synthetic crosshole GPR data through the velocity model in Figure 3a using 0.8-m-long, finite-length antennas with $v_{ant} = 0.09$ m/ns, which is 1.5 times the average subsurface velocity of 0.06 m/ns. These parameters, along with

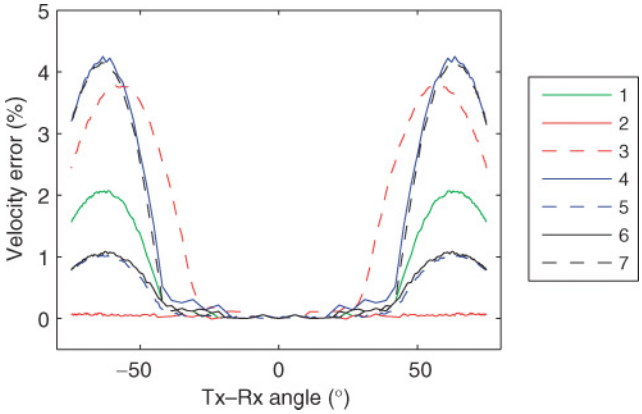

Figure 2. Velocity error versus transmitter-receiver angle (measured from the horizontal) determined from numerical simulations of finite antennas in a homogeneous medium having $\kappa = 25$. (1) $v_{ant}/v_{med} = 1.5$, borehole separation = 4 m, antenna length = 0.8 m; (2) $v_{ant}/v_{med} = 1.0$; (3) $v_{ant}/v_{med} = 2.0$; (4) borehole separation = 2 m; (5) borehole separation = 8 m; (6) antenna length = 0.4 m; (7) antenna length = 1.6 m.

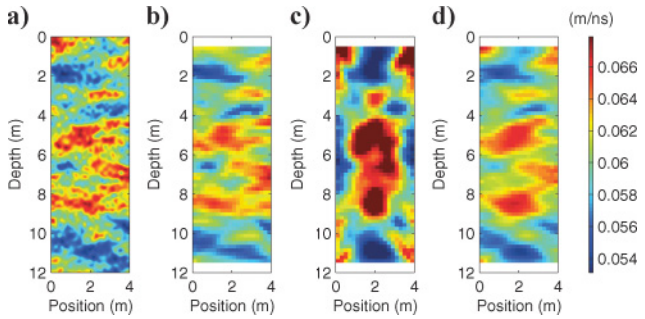

Figure 3. Heterogeneous medium example: (a) true velocity model; (b) velocity tomogram obtained from synthetic data created using point dipole antennas; (c) velocity tomogram obtained from synthetic data created using realistic, finite-length antennas; (d) velocity tomogram obtained from aperture-limited, finite-antenna data, where rays at angles greater than 40° from the horizontal were discarded.

the borehole separation of 4 m, are the same as those used to create the green curve in Figure 2. Figure 3c shows the tomogram obtained from the finite-length antennas data. Here, the tomogram is dominated by inversion artifacts to the extent that no reliable information about the subsurface can be inferred. As in Figure 3b, rays at all available angles were included in this inversion. It is the velocity errors associated with the high-angle rays, resulting from the incorrect assumption about first-arriving energy, that cause the severe artifacts seen in Figure 3c.

Figure 3d clearly illustrates the impact of the velocity errors at high transmitter-receiver angles on the tomogram. For this figure, all rays at angles greater than 40° from the horizontal were discarded from the finite-length antennas data before inversion. We now obtain a reasonable tomographic image because we avoid the errors associated with the high-angle rays. However, the resolution of this image is reduced when compared to Figure 3b because of the decreased angular aperture. For many applications, this loss of resolution may be critical. To further quantify the accuracy of the recovered velocity models in Figure 3d and b, we calculated the rms error between each tomogram and the true velocity model (Figure 3a). Figure 3b has an rms velocity error of 1.1×10^{-3} m/ns, whereas the rms error for Figure 3d is greater, at 1.5×10^{-3} m/ns.

CONCLUSIONS

Through numerical modeling we have shown that, at high propagation angles between the transmitter and receiver antennas in crosshole GPR tomography, energy traveling between the tips of the antennas can often arrive before that traveling between their centers. This can occur in both the vadose and saturated zones and contradicts the assumption of present inversion strategies that first-arriving energy always travels directly between antenna centers. Consequently, significant errors in tomographic velocity estimates can result when high-angle ray data are included in inversions. These errors are greatest for small borehole separations and lower-frequency antennas.

We stress that the results shown here are not restricted to perfectly electrically conducting (PEC) antennas. As stated, moderate resistive loading along the antennas was included for all of the examples presented, such that the modeled waveforms were similar to those we have recorded with our commercial borehole GPR system. However, we acknowledge that greater resistive loading in a progressive manner toward the ends of the antennas would likely reduce the magnitude of the errors shown here since antennas loaded in this manner tend to act as very short dipoles. To our knowledge, this type of resistive loading is uncommon in commercial borehole GPR antennas because it does not permit sufficient energy transfer into the ground.

Finally, we do not suggest that all difficulties associated with high-angle ray data in crosshole GPR tomography are related to the assumption that first-arriving energy travels directly between the antenna centers. There are lower S/N ratios associated with these data that will contribute to greater picking errors and thus less accurate inversion results as well. However, the errors resulting from the assumption about first-arriving energy can, alone, have a major impact on the quality of tomograms obtained from crosshole GPR data. Now that we understand the effect of the antennas on inversion results, finding a way to properly include the high-angle ray data becomes a feasible and important objective for future research.

ACKNOWLEDGMENTS

This research was supported by funding to R. K. from the National Science Foundation, grant EAR-0229896-002. J. I. was also supported during this work through a Departmental Chair's Fellowship at Stanford University. The authors thank Steve Arcone and an anonymous reviewer for suggestions that improved this manuscript.

REFERENCES

Alumbaugh, D., and P. Y. Chang, 2002, Estimating moisture contents in the vadose zone using cross-borehole ground-penetrating radar: A study of accuracy and repeatability: Water Resources Research, **38**, 1309, doi:10.1029/2001WR000754.

Deutsch, C. V., and A. G. Journel, 1992, GSLIB: Geostatistical software library and user's guide: Oxford University Press.

Fullagar, P. K., D. W. Livelybrooks, P. Zhang, and A. J. Calvert, 2000, Radio tomography and borehole radar delineation of the McConnell nickel sulphide deposit, Sudbury, Ontario, Canada: Geophysics, **65**, 1920–1930.

Holliger, K., and T. Bergmann, 2002, Numerical modeling of borehole georadar data: Geophysics, **67**, 1249–1257.

King, R. W. P., and G. S. Smith, 1981, Antennas in matter: Fundamentals, theory, and applications: MIT Press.

King, R. W. P., B. S. Trembly, and J. W. Strohbehn, 1983, The electromagnetic field of an insulated antenna in a conducting or dielectric medium: IEEE Transactions on Microwave Theory and Techniques, **MTT-31**, 574–583.

Moran, M. L., and R. J. Greenfield, 1993, Radar signature of a 2.5-D tunnel: Geophysics, **58**, 1573–1587.

Olsson, O., L. Falk, O. Forslund, L. Lundmark, and E. Sandberg, 1992, Borehole radar applied to the characterization of hydraulically conductive fracture zones in crystalline rock: Geophysical Prospecting, **40**, 104–116.

Peterson, J. E., 2001, Pre-inversion corrections and analysis of radar tomographic data: Journal of Environmental and Engineering Geophysics, **6**, 1–18.

Rector, J. W., and J. K. Washbourne, 1994, Characterization of resolution and uniqueness in crosswell direct-arrival traveltime tomography using the Fourier projection-slice theorem: Geophysics, **59**, 1642–1649.

Tronicke, J., K. Holliger, W. Barrash, and M. D. Knoll, 2004, Multivariate analysis of cross-hole georadar velocity and attenuation tomograms for aquifer zonation: Water Resources Research, **40**, W01519, doi:10.1029/2003WR002031.